



THE UNIVERSITY OF TOKYO
Research Center for the Early Universe

RESCEU-10/96
UTAP-229/96

Semi-analytic predictions for statistical properties of X-ray clusters of galaxies in cold dark matter universes

TETSU KITAYAMA¹ AND YASUSHI SUTO^{1,2}

¹ *Department of Physics, School of Science, The University of Tokyo, Tokyo 113, Japan.*

² *Research Center For the Early Universe (RESCEU), School of Science, The University of Tokyo, Tokyo 113, Japan.*

e-mail: kitayama@utaphp1.phys.s.u-tokyo.ac.jp, suto@phys.s.u-tokyo.ac.jp

Received 1996 March 13; accepted 1996 April 16

Abstract

Temperature and luminosity functions of X-ray clusters are computed semi-analytically, combining a simple model for the cluster gas properties with the distribution functions of halo formation epochs proposed by Lacey & Cole (1993) and Kitayama & Suto (1996). In contrast to several previous approaches which apply the Press–Schechter mass function in a straightforward manner, our method can explicitly take into account the temperature and luminosity evolution of clusters. In order to make quantitative predictions in a specific cosmological context, we adopt cold dark matter (CDM) universes.

Assuming the baryon density parameter $\Omega_B = 0.0125h^{-2}$ (h is the Hubble constant in units of $100\text{km}\cdot\text{sec}^{-1}\cdot\text{Mpc}^{-1}$) and the *COBE* normalization of matter fluctuations, temperature and luminosity functions of X-ray clusters depend sensitively on the density parameter Ω_0 . Allowing for several uncertainties in observational data as well as in our simplified assumptions, we conclude that $\Omega_0 \sim 0.2 - 0.5$ and $h \sim 0.7$ CDM models with/without the cosmological constant reproduce simultaneously the observed temperature and luminosity functions of X-ray clusters at redshift $z \sim 0$.

Subject headings: cosmology: theory – dark matter – galaxies: clusters – galaxies: formation – X-rays: galaxies

1 Introduction

Since clusters of galaxies are the largest virialized structure in the universe, they should retain the initial conditions at their formation epochs fairly faithfully. This implies that detailed studies of the clusters at high redshifts, as well as at present, should provide important clues to the evolution of the universe itself. Since X-ray identifications of clusters of galaxies are largely free from the projection effect which notoriously plagues optically selected cluster catalogues, X-ray observations are suitable for probing cosmological signatures from clusters of galaxies. Homogeneous samples of distant clusters of galaxies, which recent X-ray satellites such as *ROSAT* and *ASCA* are constructing, will uncover various statistical properties of clusters with higher reliability in the near future. Therefore, quantitative theoretical predictions are of great value in interpreting the observed data properly.

Most theoretical approaches in X-ray cosmology rely on either state-of-the-art numerical simulations, or simplified analytical formalisms. The former approach is limited by the dynamical range available on the present computer resources; a typical core radius of clusters is ($0.1 \sim 0.2h^{-1}\text{Mpc}$) while the mean separation of the Abell clusters (richness class 1) is $\sim 55h^{-1}\text{Mpc}$, where h is the Hubble constant H_0 in units of $100\text{km} \cdot \text{sec}^{-1} \cdot \text{Mpc}^{-1}$. A small-scale resolution much below the core size is essential because a large fraction of the X-ray luminosity of clusters comes from the core. On the other hand, a large simulation box size is a prerequisite for statistical studies of clusters. Unfortunately, it is still hard to simultaneously satisfy these requirements even with the currently most advanced simulations (e.g. Kang et al. 1994; Bryan et al. 1994; Cen et al. 1995).

A major fraction of the X-ray luminosity from clusters is produced via a fairly simple process, thermal bremsstrahlung. Thus one may readily compute their temperature and luminosity functions at redshift z , $n_T(T, z)$ and $n_L(L, z)$, once the mass function $n_M(M, z)$ is given, where T , L and M are the temperature, luminosity and mass of the clusters, respectively. Although the Press–Schechter theory (Press & Schechter 1974, hereafter PS) is frequently applied for this purpose, it has a serious limitation in predicting the temperature and luminosity functions; PS theory predicts the number density of virialized objects of mass M collapsed *before* a given epoch z , but does not specify the formation epoch z_f of the objects. In fact, the predictions of the spherical nonlinear collapse model (e.g. Peebles 1980) suggest that the temperature and luminosity of objects that virialize at z_f should scale as $T(z_f) \propto (1+z_f)$ and $L(z_f) \propto (1+z_f)^{7/2}$ in the Einstein–de Sitter universe, for instance. The previous approaches based on the PS formula (e.g. Evrard & Henry 1991; Hanami 1993) have simply replaced z_f by z in computing T and L (see also eq. [2.3] below). This procedure corresponds to implicitly assuming that T and L of individual clusters *decline* with time as $T(z)/T(z_f) = (1+z)/(1+z_f)$ and $L(z)/L(z_f) = (1+z)^{7/2}/(1+z_f)^{7/2}$. Numerical simulations, on the contrary, suggest modest evolution in the opposite direction (e.g. Evrard 1990; Sugimotohara 1994; Navarro, Frenk, & White 1995). While the above assumptions may not alter $n_T(T, z)$ and $n_L(L, z)$ for larger clusters most of which would have formed only recently ($z_f \sim z \ll 1$), it is likely to affect the results for less massive clusters.

This line of consideration motivates us to specify explicitly the formation epoch of virialized structures and their subsequent evolution in making statistical predictions for comparison with observations. A key quantity for this purpose is a distribution function of halo formation epochs proposed by Lacey & Cole (1993, hereafter LC) and Kitayama & Suto (1996, hereafter KS) in a similar but slightly different manner (see also Blain & Longair 1993; Sasaki 1994). In this paper, we combine these distribution functions with a simple model of cluster gas properties to make quantitative predictions on the temperature and luminosity functions of clusters of galaxies in cold dark matter (CDM) universes with/without a cosmological

constant λ_0 .

The plan of this paper is as follows. Section 2 outlines the formalism we use in computing the temperature and luminosity functions. Section 3 describes a model of X-ray clusters, and our main results are presented in Section 4. Finally, Section 5 summarizes our conclusions.

2 Formulation

2.1. Temperature and luminosity functions

The temperature function $n_T(T, z)$ of X-ray clusters is defined as the differential comoving number density of clusters of temperature T at a given redshift z (the luminosity and mass functions, $n_L(L, z)$ and $n_M(M, z)$, are defined in a similar manner). On the basis of the spherical collapse model (see Section 3.1 and Appendix A), we assume that the temperature T and the luminosity L of X-ray clusters are determined by the mass M , the redshift of formation z_f and the redshift of observation z ; i.e. $T = T(M, z_f, z)$ and $L = L(M, z_f, z)$. Then a proper theoretical prediction for $n_T(T, z)$ and $n_L(L, z)$ requires a quantity $F(M, z_f; z)$, the number density of objects of mass M which *formed* at z_f and are *observed* at z , rather than simply a mass function $n_M(M, z)$. This is because T and L depend not only on M and z but also on z_f . Once $F(M, z_f; z)$ is given, the temperature and luminosity functions are written respectively as

$$n_T(T, z) = \int_z^\infty dz_f F(M, z_f; z) \left. \frac{dM}{dT} \right|_{M=M(T, z_f, z)}, \quad (2.1)$$

and

$$n_L(L, z) = \int_z^\infty dz_f F(M, z_f; z) \left. \frac{dM}{dL} \right|_{M=M(L, z_f, z)}. \quad (2.2)$$

By contrast, conventional approaches simply translate the PS mass function as (e.g. Evrard & Henry 1991; Hanami 1993)

$$n_T(T, z) = n_{\text{PS}}(M, z) \left. \frac{dM}{dT} \right|_{M=M(T, z)}, \quad n_L(L, z) = n_{\text{PS}}(M, z) \left. \frac{dM}{dL} \right|_{M=M(L, z)}, \quad (2.3)$$

which correspond to assuming that each cluster forms when it is observed ($z_f = z$). In the above, the PS mass function $n_{\text{PS}}(M, z)$ is given by

$$n_{\text{PS}}(M, z) = \sqrt{\frac{2}{\pi}} \frac{\rho_0}{M} \frac{\delta_c(z)}{\sigma^2(M)} \left| \frac{d\sigma(M)}{dM} \right| \exp \left[-\frac{\delta_c^2(z)}{2\sigma^2(M)} \right], \quad (2.4)$$

where ρ_0 ($\simeq 2.78 \times 10^{11} \Omega_0 h^2 \text{M}_\odot \text{Mpc}^{-3}$) is the mean comoving density of the universe, $\sigma^2(M)$ is the mass variance of linear density fluctuations at the present epoch, and $\delta_c(z)$ is the critical linear overdensity evaluated at present for a spherical perturbation to collapse at z . In what follows, $\sigma^2(M)$ and $\delta_c(z)$ are computed according to the formulae presented in Appendices A and B.

Since the conventional PS approach (eq. [2.3]) identifies the epoch of formation z_f with that of observation z , the temperature and luminosity evolution of individual clusters after their formation are not properly taken into account. Our method (eqs [2.1] and [2.2]), on the other hand, can in principle include the evolution more naturally. For this purpose, one needs an appropriate expression for $F(M, z_f; z)$, as well as an evolution model which specifies $T = T(M, z_f, z)$ and $L = L(M, z_f, z)$. We will discuss these points in §2.2 and §3.1 below.

2.2. Distribution function of halo formation epochs

In the hierarchical clustering scenario, each halo increases its mass via major mergers and steady accretion, and thus the formation epoch z_f of a halo is not always well-defined. LC proposed a differential distribution function of halo formation epochs, $\partial p/\partial z_f$, defined via the probability that a halo of mass M which exists at z has a mass greater than $M/2$ for the first time at z_f (see LC §2.5.2):

$$\frac{\partial p}{\partial z_f}(M, z_f, z) = \frac{\partial p}{\partial \tilde{\omega}_f}(M, \tilde{\omega}_f) \frac{\partial \tilde{\omega}_f}{\partial z_f}, \quad (2.5)$$

$$\frac{\partial p}{\partial \tilde{\omega}_f}(M, \tilde{\omega}_f) = \frac{1}{\sqrt{2\pi}} \int_0^1 d\tilde{S} \frac{M}{M'(\tilde{S})} \frac{1}{\tilde{S}^{3/2}} \left(1 - \frac{\tilde{\omega}_f^2}{\tilde{S}}\right) \exp\left(-\frac{\tilde{\omega}_f^2}{2\tilde{S}}\right), \quad (2.6)$$

where

$$\tilde{\omega}_f(M, z_f, z) \equiv \frac{\delta_c(z_f) - \delta_c(z)}{\sqrt{\sigma^2(M/2) - \sigma^2(M)}}, \quad (2.7)$$

$$\tilde{S}(M', M) \equiv \frac{\sigma^2(M') - \sigma^2(M)}{\sigma^2(M/2) - \sigma^2(M)}, \quad (2.8)$$

and $M'(\tilde{S})$ is computed by solving equation (2.8) for M' . Figure 1 shows $\partial p/\partial z_f$ as a function of z_f in CDM models with $\lambda_0 = 0$, $h = 0.7$ and $b = 1$, where b is the bias parameter defined by $b \equiv 1/\sigma(8h^{-1}\text{Mpc})$.

Note that, in the above definition of the halo formation epochs, the mass of a halo at z_f and z is different at most by a factor of 2. Supposedly this factor will be close to 2, since the increase of halo masses is expected to be dominated by steady accretion of small objects (although the mass increase is not necessarily continuous because of major mergers, the fraction of such events should be relatively small). Thus the LC proposal implies that the quantity $F(M, z_f; z)$ in equations (2.1) and (2.2) can be written as

$$F_{\text{LC}}(M, z_f; z) dM dz_f \equiv 2 \frac{\partial p}{\partial z_f}(2M, z_f, z) n_{\text{PS}}(2M, z) dM dz_f, \quad (2.9)$$

where M is the halo mass at z_f , which is assumed to have doubled by z , and $n_{\text{PS}}(M, z)$ is the PS mass function given by equation (2.4).

As discussed by LC, however, the probability $\partial p/\partial \tilde{\omega}_f$ given by equation (2.6) becomes negative for small $\tilde{\omega}_f$ in the case of power-law matter fluctuation spectra $P(k) \propto k^n$ with index $n > 0$, implying that the above definition of the halo formation distribution function is not completely self-consistent. Since the effective power index of the observed fluctuation spectrum is negative below the cluster scale (e.g. Peacock & Dodds 1994), this would not be a serious problem for most astrophysically interesting objects. Nevertheless this clearly exhibits the importance of exploring other prescriptions for computing the distribution of halo formation epochs.

One such alternative is given by KS. They derived expressions for the rates of formation and destruction of bound virialized objects based upon the conditional probability argument developed by Bond et al. (1991), Bower (1991), and LC. Their formalism yields the number density of haloes of mass $M \sim M + dM$ that form via major mergers at $z_f \sim z_f + dz_f$ and remain in the range $M \sim 2M$ at a later time z (see KS §2.4):

$$F_{\text{KS}}(M, z_f; z) dM dz_f = \frac{1}{\sqrt{2\pi}} \frac{1}{\sqrt{\sigma^2(M/2) - \sigma^2(M)}} \left\{ 2 - \left(\frac{\delta_c(z_f) - 2\delta_c(z)}{\delta_c(z)} \right) \right. \\ \left. \times \exp \left[\frac{2\delta_c(z) \{ \delta_c(z_f) - \delta_c(z) \}}{\sigma^2(M)} \right] \text{erfc}[X(M, z_f, z)] \right.$$

$$-\operatorname{erfc}[Y(M, z_f, z)] \left\} \left[\frac{d\delta_c(z_f)}{dz_f} \right] n_{\text{PS}}(M, z_f) dM dz_f, \quad (2.10)$$

where $\operatorname{erfc}(u)$ is the complimentary error function defined by

$$\operatorname{erfc}(u) \equiv \frac{2}{\sqrt{\pi}} \int_u^\infty \exp(-t^2) dt, \quad (2.11)$$

and $X(M, z_f, z)$ and $Y(M, z_f, z)$ are respectively

$$X(M, z_f, z) \equiv \frac{\sigma^2(2M)[\delta_c(z_f) - 2\delta_c(z)] + \sigma^2(M)\delta_c(z)}{\sqrt{2\sigma^2(M)\sigma^2(2M)[\sigma^2(M) - \sigma^2(2M)]}}, \quad (2.12)$$

$$Y(M, z_f, z) \equiv \frac{\sigma^2(M)\delta_c(z) - \sigma^2(2M)\delta_c(z_f)}{\sqrt{2\sigma^2(M)\sigma^2(2M)[\sigma^2(M) - \sigma^2(2M)]}}. \quad (2.13)$$

As mentioned by KS, the above definition (eq. [2.10]) for the formation epoch distribution may lead to a systematic overestimation of the number of haloes that form by mergers at z_f (see §4 of KS).

Strictly speaking, therefore, neither F_{LC} nor F_{KS} is a completely satisfactory expression for $F(M, z_f; z)$. In practice, however, F_{LC} and F_{KS} are in good agreement except at $z_f \sim z$ (Fig. 2); the small discrepancy is ascribed to different criteria of “formation” in the two approaches, because the formation epochs are not uniquely defined for haloes which increase their mass quiescently via accretion. Furthermore, as will be shown in §4, such a difference between the LC and KS models does not affect the predictions for $n_{\text{T}}(T, z)$ and $n_{\text{L}}(L, z)$ (see Figs 6 and 7). Thus we believe that they provide reasonable approximations to $F(M, z_f; z)$, at least for our present purpose.

3 Descriptions of X-ray clusters

3.1. A simple model

Given the distribution function of halo formation epochs $F(M, z_f; z)$, it remains to specify $T = T(M, z_f, z)$ and $L = L(M, z_f, z)$. We basically follow our previous model (§3.1.2 of KS), but slightly modify the hypothesis on the temperature and luminosity evolution.

We make the approximation that X-ray clusters consist of dissipationless dark matter and baryonic gas. The dark matter component dominates the total gravitating mass and is supposed to be in virial equilibrium. Once the cosmological parameters such as Ω_0 and λ_0 are specified, the virial radius r_{vir} and the virial temperature T_{vir} are determined by the mass M and the formation epoch z_f using the spherical collapse model (e.g. Peebles 1980; Appendix A) We compute these quantities from the mean density ρ_{vir} given in Appendix A by

$$r_{\text{vir}}(M, z_f) = \left(\frac{3M}{4\pi\rho_{\text{vir}}} \right)^{1/3}, \quad (3.1)$$

$$T_{\text{vir}}(M, z_f) = \frac{GM\mu m_{\text{p}}}{3k_{\text{B}}r_{\text{vir}}}, \quad (3.2)$$

where G is the gravitational constant, k_{B} is the Boltzmann constant, m_{p} is the proton mass, and μ is the mean molecular weight. Hereafter we assume that the intracluster gas is fully ionized with primordial abundances of helium and hydrogen, and thus set $\mu = 0.59$.

For a cluster temperature of $\gtrsim 3\text{keV}$, the contribution from the line emission on the total X-ray luminosity can be neglected. Since the shape and amplitude of the temperature and luminosity functions

are derived observationally for relatively high temperature clusters (see the error box in Figs 6 ~ 10 below; Henry & Arnaud 1991), we compute the X-ray luminosity only from thermal bremsstrahlung emission. Incidentally, the X-ray line emission from less massive clusters may be important in considering the origin of the soft X-ray background (Cen et al. 1995; Suto et al. 1996), and we will discuss the effect of line emissions elsewhere (Sasaki et al. 1996).

We assume that the cluster gas is isothermal with temperature given by

$$T(M, z_f, z) = \kappa(z_f, z) T_{\text{vir}}(M, z_f), \quad (3.3)$$

where $\kappa(z_f, z)$ is introduced so that temperature evolution due to quiescent accretion of matter after z_f can be taken into account. Note that this treatment is possible because our method explicitly distinguishes z_f from z . As there is not yet a good theoretical model to describe the temperature evolution, we simply suppose that $\kappa(z_f, z)$ takes a power-law form:

$$\kappa(z_f, z) = \left(\frac{1 + z_f}{1 + z} \right)^s. \quad (3.4)$$

Hydrodynamical simulations indicate that the temperature of clusters, once formed, does not change drastically after virialization, and are roughly consistent with $0 \lesssim s \lesssim 1$ (e.g. Evrard 1990; Navarro, Frenk & White 1995).

We adopt the following spherically symmetric distribution for intracluster gas density (e.g. Jones & Forman 1984)

$$\rho_{\text{gas}}(r) = \rho_{\text{gas}}^0 \left[1 + \left(\frac{r}{r_c} \right)^2 \right]^{-1}, \quad (3.5)$$

where ρ_{gas}^0 is the central gas density, and r_c is the core radius. Since this is basically an empirical fitting formula, it is difficult to predict r_c . Thus we adopt a simple self-similar model in which r_c is proportional to $r_{\text{vir}}(M, z_f)$:

$$r_c = 0.15 h^{-1} \text{Mpc} \times \frac{r_{\text{vir}}(M, z_f)}{r_{\text{vir}}(10^{15} M_{\odot}, z_f = 0)} \quad (3.6)$$

where the normalization is chosen to match the X-ray observations (Abramopoulos & Ku 1983; Jones & Forman 1984). Now ρ_{gas}^0 is fixed by the relation:

$$\int_0^{r_{\text{vir}}} \rho_{\text{gas}}(r) 4\pi r^2 dr = M \left(\frac{\Omega_{\text{B}}}{\Omega_0} \right), \quad (3.7)$$

where Ω_{B} is the baryonic density parameter of the universe chosen to be consistent with primordial nucleosynthesis: $\Omega_{\text{B}} = 0.0125 h^{-2}$ (Walker et al. 1991). We assume no intrinsic evolution for the gas density profile, which is also suggested by numerical simulations (e.g. Navarro, Frenk & White 1995).

Combining all the above assumptions, the temperature T and the bolometric luminosity L_{bol} of X-ray clusters in our model are roughly related to M , z_f and z as follows:

$$T(M, z_f, z) \propto M^{2/3} (1 + z_f)^{\xi} \left(\frac{1 + z_f}{1 + z} \right)^s \quad (3.8)$$

$$L_{\text{bol}}(M, z_f, z) \propto M^{4/3} (1 + z_f)^{7\xi/2} \left(\frac{1 + z_f}{1 + z} \right)^{s/2}, \quad (3.9)$$

where ξ is the effective index which varies weakly with z_f , Ω_0 and λ_0 ; e.g. $\xi = 1$ independent of z_f in the case of $(\Omega_0, \lambda_0) = (1, 0)$, while $\xi \simeq 0.5$ at $z_f \sim 0$ and $\xi \simeq 1$ at $z_f \gtrsim 2$ for $(\Omega_0, \lambda_0) = (0.2, 0.8)$.

3.2. Comparison with observed correlations

The model presented in the previous subsection is admittedly crude, so we need to examine the extent to which it is consistent with the available observations before presenting the results for $n_T(T, z)$ and $n_L(L, z)$. Specifically, we plot the correlations among T , r_c and $L(2 - 10\text{keV})$ in Figures 3, 4 and 5. In these figures we select three representative CDM models, Eh5, L3h7, and O3h7, which have respectively $(\Omega_0, \lambda_0, h) = (1.0, 0, 0.5)$, $(0.3, 0.7, 0.7)$, and $(0.3, 0, 0.7)$. In fact, model L3h7 is shown to be reasonably consistent with the observed temperature and luminosity functions at $z = 0$ in the next section.

Basically, our models reproduce fairly well the observed $T - r_c$ and $L(2 - 10\text{keV}) - r_c$ correlations, considering that most clusters present at $z = 0$ would have formed at $z_f \lesssim 1$. The slopes of our models in Figures 3 and 4 would become less steep if the distribution of z_f is taken into account, because massive clusters (large T and L) are likely to have formed more recently than less massive ones. As regards the $L(2 - 10\text{keV}) - T$ correlation on the other hand, only low Ω_0 models show reasonable agreement with the observed data at large L and T . The predicted curves are less steep than the observed one. In fact, several authors have pointed out that simple adiabatic models fail to account for the observed $L - T$ relation (e.g. Navarro, Frenk & White 1995). It has also been suggested that the discrepancy may possibly be reconciled if the gas has attained large entropy at high redshift (Kaiser 1991; Evrard 1990; Evrard & Henry 1991).

Apparently this is an important area of research, especially if one takes seriously the above discrepancy between the observed $L - T$ relation and the theoretical prediction of a simple adiabatic model. Nevertheless it is fairly independent of our current formalism; once any physical model of such pre-heating specifies $T = T(M, z_f, z)$ and $L = L(M, z_f, z)$, then we can compute the resulting $n_T(T, z)$ and $n_L(L, z)$ by a straightforward application of the method described here. Thus we do not discuss this problem further and hope to come back to it elsewhere.

4 Predictions for temperature and luminosity functions

The temperature and luminosity functions of clusters predicted in CDM universes at $z = 0$ are shown in Figures 6 and 7, respectively. All the models adopt $h = 0.7$ based on the recent observations of Cepheids by the Hubble Space Telescope (Tanvir et al. 1995). The fluctuation amplitudes are normalized according to the *COBE* 2 year data (Gorski et al. 1995; Sugiyama 1995). Panels (a) and (b) in these figures are based on the LC model (eq. [2.9]) while panels (c) and (d) adopt the KS model (eq. [2.10]). The comparison implies that the results are quite insensitive to the choice of models, because the small difference between the two models shown in Figure 2 has been canceled out in the integration over z_f (eqs [2.1] [2.2]). Thus in what follows we will adopt the LC model just for definiteness. Clearly the predictions of the temperature and luminosity functions vary largely with the shape and the amplitude of the fluctuation spectrum. Since both of these are fixed by Ω_0 and λ_0 assuming the CDM model and the *COBE* normalization, comparison of the theoretical predictions with the observed temperature and luminosity functions serves as a possible discriminator of the values of Ω_0 and λ_0 .

We have tested the robustness of the above predictions against our assumptions about the temperature evolution in Figure 8. The temperature functions depend rather sensitively on the evolution index s . In fact, the temperature evolution assumed in our model, $T(z)/T(z_f) = (1 + z_f)^s / (1 + z)^s$ with $s = 1$ (thick lines), tends to move the predictions of $n_T(T, z = 0)$ to the right roughly by a factor of $(1 + z_f)$ relative to the $s = 0$ case (thin lines). Although the formation epoch z_f varies with M and therefore with T of an individual cluster, $\langle z_f \rangle \sim 0.5$ for typical clusters reasonably accounts for the behavior in Figure 8a.

On the other hand, the shift in the luminosity function is rather small (Figure 8b), because our evolution model assumes that the cluster density is fairly constant after virialization and the bolometric luminosity evolves as $L_{\text{bol}}(z)/L_{\text{bol}}(z_f) = (1+z_f)^{s/2}/(1+z)^{s/2}$.

Incidentally, Figure 8 shows that our $s = 0$ model prediction is very close to the original PS approach (eq. [2.3]), especially for the temperature function. However, this does not imply that the effect of $z_f \neq z$ is negligible. Our predictions have been shifted relative to the original PS approach in the following two ways. One is the horizontal shift due to the different hypotheses for the temperature and luminosity evolution; the original PS approach implicitly assumes for instance $T(z)/T(z_f) = (1+z)/(1+z_f)$ and $L(z)/L(z_f) = (1+z)^{7/2}/(1+z_f)^{7/2}$ in the $\Omega_0 = 1$ universe, while we assume those just mentioned in the last paragraph. The other is the vertical shift due to the different mass of haloes at z_f and at z ; our formalism assumes that the mass of a halo at z_f is half of that at z , while no mass change is considered in the original PS approach. The former shift depends on the evolution index s , and the latter one is sensitive to the fluctuation spectral index. On cluster scales, the above effects have almost canceled each other for the temperature function with $s = 0$.

In any case, Figures 6, 7 and 8 indicate that, with the *COBE* normalization, a change in the parameter s in the range $0 \lesssim s \lesssim 1$ roughly corresponds to changing Ω_0 by $0.1 \sim 0.2$. In the case of $s = 0$ and $h = 0.7$, either the $(\Omega_0, \lambda_0) \simeq (0.4, 0.6)$ or the $(0.5, 0)$ CDM model fit best within the observational error box. If $s = 1$ is adopted instead, models with $(\Omega_0, \lambda_0) \simeq (0.3, 0.7)$ or $(0.4, 0)$ are preferred. Of course, the conventional argument of the age problem also points to a lower Ω_0 ; if $h = 0.7$ as we adopted here, the ages of the universe are 13.5 Gyr, 12.4 Gyr, 10.9 Gyr and 10.5 Gyr for $(\Omega_0, \lambda_0) = (0.3, 0.7)$, $(0.4, 0.6)$, $(0.4, 0)$ and $(0.5, 0)$ respectively.

Adopting the *COBE* normalization in the computation of the temperature and luminosity functions, we implicitly assume that luminous clusters trace the underlying mass distribution. Although this seems quite reasonable on scales relevant for formation and clustering of galaxy clusters, it is not easy to rigorously justify this assumption. So we change the normalization of the fluctuations and plot the results for $b = 1.5$ and 0.5 in Figure 9 (assuming $s = 0.5$). For comparison, the *COBE* 2 year data imply that $b = 0.73, 0.87$, and 1.8 in models Eh5, L3h7 and O3h7 respectively.

With the above uncertainty and the observational error in mind, an acceptable range of Ω_0 from the observed temperature and luminosity functions is $0.2 \lesssim \Omega_0 \lesssim 0.4$ in the case of spatially flat CDM universe, and $0.3 \lesssim \Omega_0 \lesssim 0.5$ for open CDM universe. It should be noted that the $\Omega_0 = 1$ CDM model fails to account for the observation by a wide margin and can be ruled out even from the present comparison only.

More interesting for the future X-ray observations are the predictions of evolutionary behaviors in the temperature and luminosity functions. Figure 10 plots the predictions at $z = 0$ and 1 . Evolution of the temperature function (Figure 10a) is in general negative (i.e. decreasing number density toward the past) for massive clusters (large T), while it becomes positive for smaller ones. In model L3h7, for instance, a significant negative evolution occurs at $T \gtrsim 2\text{keV}$, where observed data are available at $z \sim 0$. On the other hand, the luminosity function mostly shows very weak evolution in the range of observational interest (Figure 10b). This is still consistent, within the observational error bar, with the results by Gioia et al. (1990) which indicate weakly negative evolution at $L(0.3 - 3.5\text{keV}) \gtrsim 10^{44} h^{-2} \text{erg s}^{-1}$. Our model can be tested against future observations through the different evolutionary signature of $n_{\text{T}}(T, z)$ (negative evolution) and $n_{\text{L}}(L, z)$ (almost no evolution).

5 Conclusions

We have examined statistical properties of X-ray clusters in CDM universes in a semi-analytic manner, which is complementary to numerical simulations. Our method is different from the previous approaches based upon the conventional PS theory (e.g. Evrard & Henry; Hanami 1993), in that we explicitly took account of the epochs of cluster formation adopting the halo formation epoch distributions proposed by LC and KS. As a result, our method can include the subsequent evolution of cluster temperature and luminosity.

Although the LC and KS proposals involve slightly different definitions of the halo formation epochs, we found that the resultant temperature and luminosity functions are remarkably similar. Deviations from the previous PS approach become larger for clusters that form at higher redshift and for stronger evolution.

The shape and amplitude of the temperature and luminosity functions vary sensitively with the cosmological density parameter Ω_0 , if the fluctuation amplitude is fixed by the *COBE* normalization. Given the qualitative nature of our simple model, however, we should not constrain the cosmological parameters so stringently. Rather we conclude that the low-density $\Omega_0 \sim 0.2 - 0.5$ CDM models with/without the cosmological constant are roughly consistent with the observed temperature and luminosity functions. Nevertheless we can argue against $\Omega_0 = 1$ CDM models at least from the present analysis only.

We thank Takahiro T. Nakamura and Naoshi Sugiyama for useful discussions on the spherical collapse model and the *COBE* normalization. We are grateful to Ewan D. Stewart for a careful reading of the manuscript. This research was supported in part by the Grants-in-Aid by the Ministry of Education, Science and Culture of Japan (07740183, 07CE2002).

APPENDICES

A Spherical collapse in $\Omega_0 \leq 1$ universes

In the present analysis, we need the mean density $\rho_{\text{vir}}(z_f)$ and the critical linear overdensity $\delta_c(z_f)$ of an object that virializes at z_f in a universe with arbitrary Ω_0 ($\Omega \leq 1$). For definiteness, we summarize the results of the spherical collapse model as well as the fitting formula we used for $\lambda_0 = 1 - \Omega_0$ models (Peebles 1980; Lahav et al. 1991; LC; Nakamura 1996). Note that δ_c given below is the value computed at virialization, and $\delta_c(z_f)$ used in our main text is the value computed at present. They are related via $\delta_c(z_f) \equiv \delta_c \cdot D(z_f = 0)/D(z_f)$, where $D(z)$ is the linear growth rate.

1. $\Omega_0 = 1$,

$$\frac{\rho_{\text{vir}}(z_f)}{\bar{\rho}(z_f)} = 18\pi^2 \simeq 178, \quad (\text{A.1})$$

$$\delta_c = \frac{3(12\pi)^{2/3}}{20} \simeq 1.69, \quad (\text{A.2})$$

2. $\Omega_0 < 1, \lambda_0 = 0$,

$$\frac{\rho_{\text{vir}}(z_f)}{\bar{\rho}(z_f)} = 4\pi^2 \frac{(\cosh \eta_f - 1)^3}{(\sinh \eta_f - \eta_f)^2}, \quad (\text{A.3})$$

$$\delta_c = \frac{3}{2} \left[\frac{3 \sinh \eta_f (\sinh \eta_f - \eta_f)}{(\cosh \eta_f - 1)^2} - 2 \right] \left[1 + \left(\frac{2\pi}{\sinh \eta_f - \eta_f} \right)^{2/3} \right], \quad (\text{A.4})$$

3. $\Omega_0 < 1, \lambda_0 = 1 - \Omega_0$,

$$\begin{aligned} \frac{\rho_{\text{vir}}(z_f)}{\bar{\rho}(z_f)} &= \left(\frac{r_{\text{ta}}}{r_{\text{vir}}} \right)^3 \frac{2w_f}{\chi}, \\ &\simeq 18\pi^2 (1 + 0.4093w_f^{0.9052}), \end{aligned} \quad (\text{A.5})$$

$$\begin{aligned} \delta_c &= \frac{3}{5} F \left(\frac{1}{3}, 1, \frac{11}{6}; -w_f \right) \left(\frac{2w_f}{\chi} \right)^{1/3} \left(1 + \frac{\chi}{2} \right), \\ &\simeq \frac{3(12\pi)^{2/3}}{20} (1 + 0.123 \log_{10} \Omega_f), \end{aligned} \quad (\text{A.6})$$

In the above, $\bar{\rho}(z_f) \equiv \rho_0(1 + z_f)^3$, $\eta_f \equiv \text{arccosh}(2/\Omega_f - 1)$, $w_f \equiv 1/\Omega_f - 1$, $\chi \equiv \lambda_0 H_0^2 r_{\text{ta}}^3 / (GM)$, r_{ta} is the maximum turn-around radius and F is the hyper-geometric function of type (2,1). The density parameter Ω_f is defined at z_f and is related to Ω_0 and λ_0 through

$$\Omega_f = \frac{\Omega_0(1 + z_f)^3}{\Omega_0(1 + z_f)^3 + (1 - \Omega_0 - \lambda_0)(1 + z_f)^2 + \lambda_0}. \quad (\text{A.7})$$

B Mass variance for the CDM fluctuation spectrum

The mass variance $\sigma^2(M)$ is related to the linear power spectrum of density fluctuations $P(k)$ through

$$\sigma^2(M) = \frac{1}{(2\pi)^3} \int_0^\infty P(k) W^2(kr_M) 4\pi k^2 dk, \quad (\text{B.1})$$

where the filtering radius r_M is related to the mass M by $r_M = [3M/(4\pi\rho_0)]^{1/3}$ as the top-hat window function is used:

$$W(x) = \frac{3}{x^3}(\sin x - x \cos x). \quad (\text{B.2})$$

We adopt the CDM power spectrum of the form given by Bardeen et al. (1986) with the scale invariant initial condition:

$$P(k) \propto k \left[\frac{\ln(1 + 2.34q)}{2.34q} \right]^2 [1 + 3.89q + (16.1q)^2 + (5.46q)^3 + (6.71q)^4]^{-1/2}, \quad (\text{B.3})$$

where $q \equiv k/(\Gamma h \text{ Mpc}^{-1})$. Here the quantity Γ for non-negligible baryon density is given by (Peacock & Dodds 1994; Sugiyama 1995)

$$\Gamma = \Omega_0 h (T_0/2.7 \text{ K})^{-2} \exp[-\Omega_B(1 + \sqrt{2h}\Omega_0^{-1})], \quad (\text{B.4})$$

where T_0 is the temperature of the cosmic microwave background radiation.

We found that σ^2 and $d\sigma^2/dM$ calculated from the above equations are accurately fitted simultaneously by the following formula and its derivative with respect to m :

$$\sigma^2 \propto [1 + 2.208m^p - 0.7668m^{2p} + 0.7949m^{3p}]^{-\frac{2}{9p}}, \quad (\text{B.5})$$

where $p = 0.0873$, and $m \equiv M(\Gamma h)^2/(10^{12} M_\odot)$. The above approximation holds within a few percent for both σ^2 and $d\sigma^2/dM$ in the range $10^{-6} \lesssim m \lesssim 10^4$. Throughout the present paper, σ is evaluated via equation (B.5) and normalized by

$$\sigma(r_M = 8h^{-1} \text{ Mpc}) = \frac{1}{b}, \quad (\text{B.6})$$

where b is the bias parameter.

C Fitting formulae for the Lacey & Cole distribution function

Since the distribution function of the halo formation epochs derived by LC (eq. [2.6]) requires a time-consuming numerical integration, the following fitting formula is used in the present paper.

First we consider the case of power-law fluctuation spectra $P(k) \propto k^n$, i.e. $\sigma^2(M) \propto M^{-\alpha}$ where $\alpha \equiv (n+3)/3$. Then equation (2.6) reduces to

$$\frac{\partial p}{\partial \tilde{\omega}_f}(\alpha, \tilde{\omega}_f) = \sqrt{\frac{8}{\pi}} e^{-\tilde{\omega}_f^2/2} - \frac{2(2^\alpha - 1)}{\sqrt{\pi}\alpha} \tilde{\omega}_f \int_{\frac{\tilde{\omega}_f}{\sqrt{2}}}^{\infty} dy \frac{e^{-y^2}}{y^2} \left(1 + \frac{2^\alpha - 1}{2} \frac{\tilde{\omega}_f^2}{y^2} \right)^{(1-\alpha)/\alpha}. \quad (\text{C.1})$$

For $\tilde{\omega}_f \ll 1$, equation (C.1) becomes

$$\begin{aligned} \frac{\partial p}{\partial \tilde{\omega}_f}(\alpha, \tilde{\omega}_f) &\simeq \sqrt{\frac{8}{\pi}} \left[1 - \frac{\sqrt{2^\alpha - 1}}{\alpha} \int_0^{\sqrt{2^\alpha - 1}} (1+x^2)^{(1-\alpha)/\alpha} dx \right] \\ &\quad + \frac{2(2^\alpha - 1)}{\alpha} \tilde{\omega}_f + O(\tilde{\omega}_f^2), \end{aligned} \quad (\text{C.2})$$

For $\tilde{\omega}_f \gg 1$, on the other hand, we found that numerical results for equation (C.1) are insensitive to α and well approximated by the solution in the $\alpha = 1$ case:

$$\frac{\partial p}{\partial \tilde{\omega}_f}(\alpha = 1, \tilde{\omega}_f) = 2\tilde{\omega}_f \operatorname{erfc} \left(\frac{\tilde{\omega}_f}{\sqrt{2}} \right). \quad (\text{C.3})$$

On the basis of equations (C.2) and (C.3), we constructed the following interpolation formula which gives a very good fit to equation (C.1):

$$\frac{\partial p}{\partial \tilde{\omega}_f}(\alpha, \tilde{\omega}_f) = \frac{A(\alpha)}{1 + B(\alpha)\tilde{\omega}_f} e^{-5\tilde{\omega}_f^2} + 2C(\alpha)\tilde{\omega}_f \operatorname{erfc}\left(\frac{\tilde{\omega}_f}{\sqrt{2}}\right), \quad (\text{C.4})$$

where

$$A(\alpha) \equiv \sqrt{\frac{8}{\pi}}(1 - \alpha)(0.0107 + 0.0163\alpha), \quad (\text{C.5})$$

$$B(\alpha) \equiv \frac{2}{A(\alpha)} \left[C(\alpha) - \frac{2^\alpha - 1}{\alpha} \right], \quad (\text{C.6})$$

$$C(\alpha) \equiv 1 - \frac{1 - \alpha}{25}. \quad (\text{C.7})$$

Since equations (C.1)–(C.3) are valid only when the underlying spectra are of power-law form, the above fitting formulae may not be applicable to more general spectra. In fact, in the case of the CDM spectrum, a straightforward substitution of the effective spectral index $\alpha_{\text{eff}} \equiv -d \ln \sigma_{\text{CDM}}^2 / d \ln M$ into equation (C.4) does not work very well, because α_{eff} varies with the mass scale and so cannot be approximated by a constant in the integral of equation (2.6). Nevertheless, we found that equation (C.4) still gives an excellent empirical fit to equation (2.6) for the CDM spectrum, if $\tilde{\alpha}_{\text{eff}}$ below is adopted rather than α_{eff} :

$$\tilde{\alpha}_{\text{eff}} \equiv \alpha_{\text{eff}}(0.6268 + 0.3058\alpha_{\text{eff}}). \quad (\text{C.8})$$

The accuracy of this approximation is within a few percent in the range $10^6 M_\odot \lesssim M(\Omega_0 h^2)^2 \lesssim 10^{16} M_\odot$ (see Fig. 11).

REFERENCES

- Abramopoulos, F., & Ku, W. 1983, *ApJ*, 271, 446
- Bardeen, J.M., Bond J.R., Kaiser, N., & Szalay, A.S. 1986, *ApJ*, 304, 15
- Blain, A.W., & Longair, M.S. 1993, *MNRAS*, 265, L21
- Bond, J.R., Cole, S., Efstathiou, G., & Kaiser, N. 1991, *ApJ*, 379, 440
- Bower, R.J. 1991, *MNRAS*, 248, 332
- Bryan, G.L., Cen, R., Norman, M.L., Ostriker, J.P., & Stone, J.M. 1994, *ApJ*, 428, 405
- Cen, R., Kang, H., Ostriker, J.P., & Ryu, D. 1995, *ApJ*, 451, 436
- David, L.P., Slyz, A., Jones, C., Forman, W., & Vrtilik, S.D. 1993, *ApJ*, 412, 479
- Edge, A.C., & Stewart, G.C. 1991a, *MNRAS*, 252, 414
- Edge, A.C., & Stewart, G.C. 1991b, *MNRAS*, 252, 428
- Evrard, A.E. 1990, *ApJ*, 363, 349
- Evrard, A.E., & Henry, J.P. 1991, *ApJ*, 383, 95
- Gioia, I.M., Henry, J.P., Maccacaro, T., Morris, S.L., Stocke, J.T., & Wolter, A. 1990, *ApJ*, 356, L35
- Gorski, K.M., Ratra, B., Sugiyama, N., & Banday, A.J. 1995, *ApJ*, 444, L65
- Hanami, H. 1993, *ApJ*, 415, 42
- Henry, J.P., & Arnaud, K.A. 1991, *ApJ*, 372, 410
- Jones, C., & Forman, W. 1984, *ApJ*, 276, 38
- Kaiser, N. 1991, *ApJ*, 383, 104
- Kang, H., Cen, R., Ostriker, J.P., & Ryu, D. 1994, *ApJ*, 428, 1
- Kitayama, T., & Suto, Y. 1996, *MNRAS*, in press (KS).
- Lacey, C.G., & Cole, S. 1993, *MNRAS*, 262, 627 (LC)
- Lahav, O., Lilje, P.B., Primack, J.R., & Rees, M.J. 1991, *MNRAS*, 251, 128
- Nakamura, T.T. 1996, Master thesis (Univ. of Tokyo, unpublished).
- Navarro, J.F., Frenk, C.S., & White, S.D.M. 1995, *MNRAS*, 275, 720
- Peacock, J.A., & Dodds, S.J. 1994, *MNRAS*, 267, 1020
- Peebles, P.J.E. 1980, *The Large-Scale Structure of the Universe*. (Princeton Univ. Press: Princeton)
- Press, W.H., & Schechter, P. 1974, *ApJ*, 187, 425
- Sarazin, C.L. 1988, *X-ray Emission from Clusters of Galaxies*. (Cambridge Univ. Press: Cambridge)
- Sasaki, S. 1994, *PASJ*, 46, 427
- Sasaki, S., Masai, K., Kitayama, T., & Suto, Y. 1996, in preparation.
- Suginohara, T. 1994, *PASJ*, 46, 441
- Sugiyama, N. 1995, *ApJS*, 100, 281
- Suto, Y. 1993, *Prog.Theor.Phys.*, 90, 1173
- Suto, Y., Makishima, K., Ishisaki, Y., & Ogasaka, Y. 1996, *ApJL*, 461, L33
- Tanvir, N.R., Shanks, T., Ferguson, H.C., & Robinson, D.R.T. 1995, *Nature*, 377, 27
- Walker, T.P., et al. 1991, *ApJ*, 376, 51

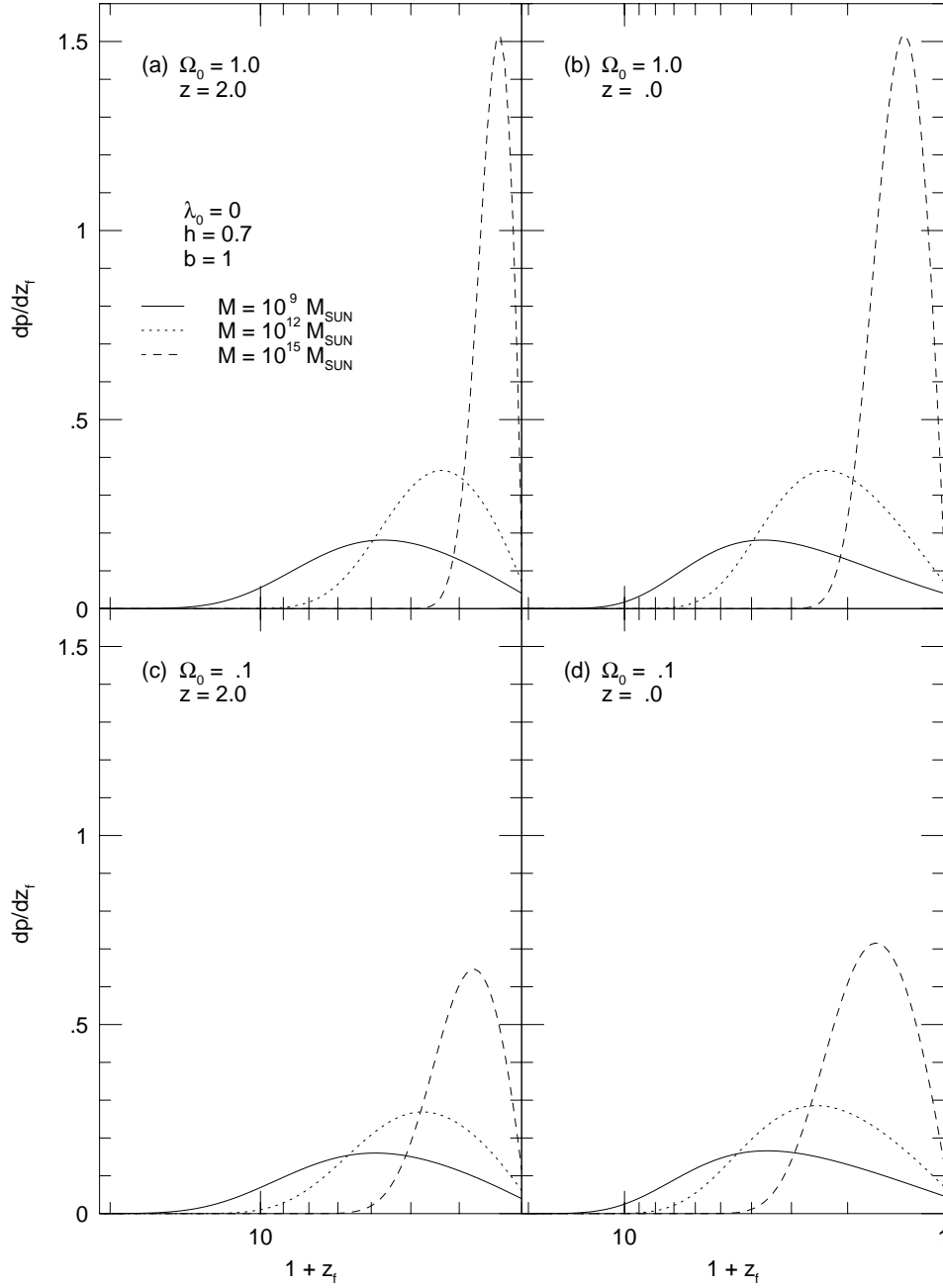


Figure 1: The formation epoch distribution function $\partial p/\partial z_f$ by LC in CDM models; (a) $\Omega_0 = 1$, $z = 2$, (b) $\Omega_0 = 1$, $z = 0$, (c) $\Omega_0 = 0.1$, $z = 2$, (d) $\Omega_0 = 0.1$, $z = 0$. In all panels, $\lambda_0 = 0$, $h = 0.7$, and $b = 1$. Lines indicate $M = 10^9 M_{\odot}$ (solid), $10^{12} M_{\odot}$ (dotted), and $10^{15} M_{\odot}$ (dashed).

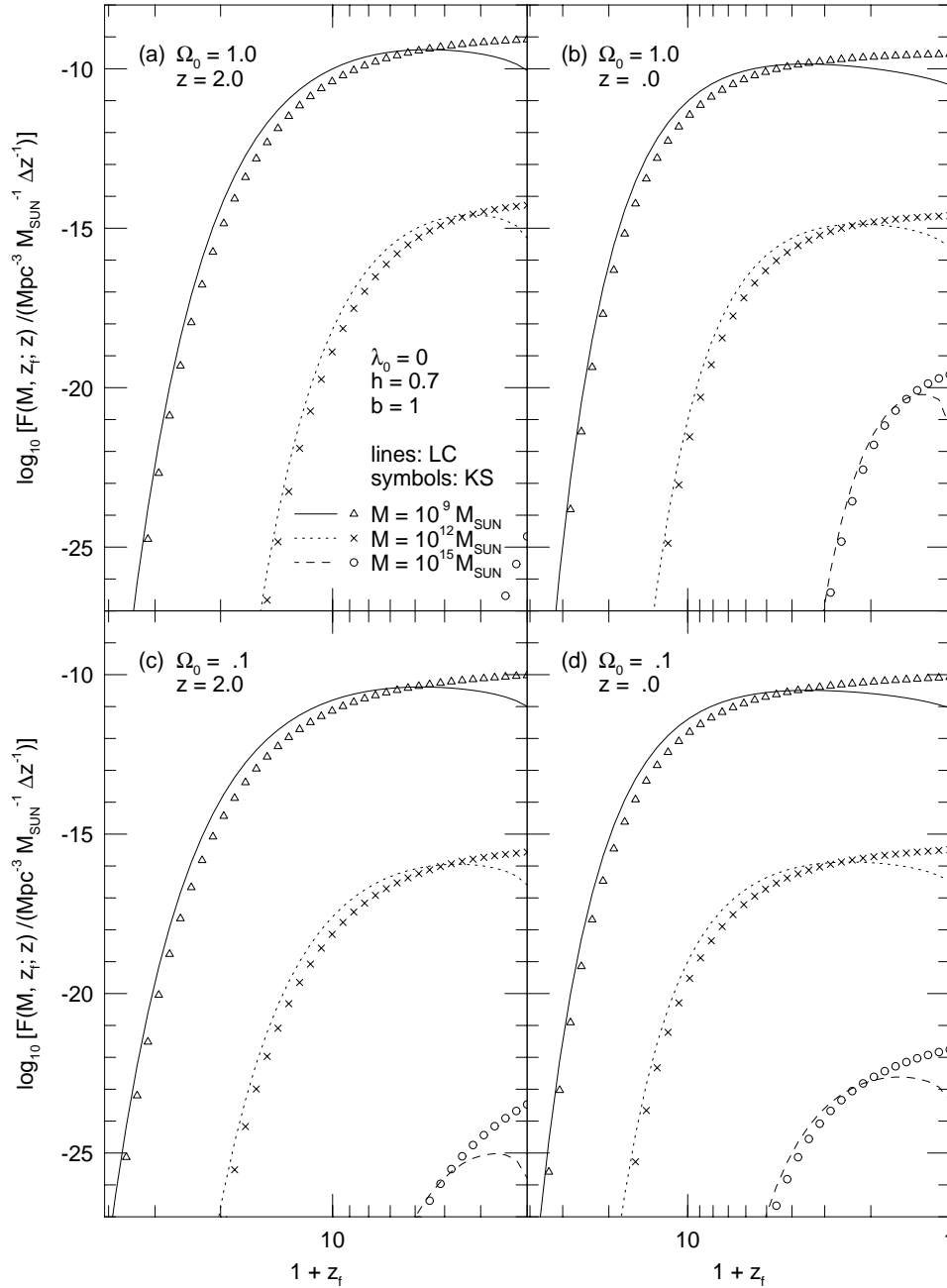


Figure 2: The distribution function of halo formation epochs by LC (eq. [2.9]) and KS (eq. [2.10]) in CDM models; (a) $\Omega_0 = 1$, $z = 2$, (b) $\Omega_0 = 1$, $z = 0$, (c) $\Omega_0 = 0.1$, $z = 2$, (d) $\Omega_0 = 0.1$, $z = 0$. In all panels, $\lambda_0 = 0$, $h = 0.7$, $b = 1$. Lines and symbols indicate the LC and KS formulae respectively for $M = 10^9 M_{\odot}$ (solid line, triangles), $10^{12} M_{\odot}$ (dotted line, crosses), and $10^{15} M_{\odot}$ (dashed line, circles).

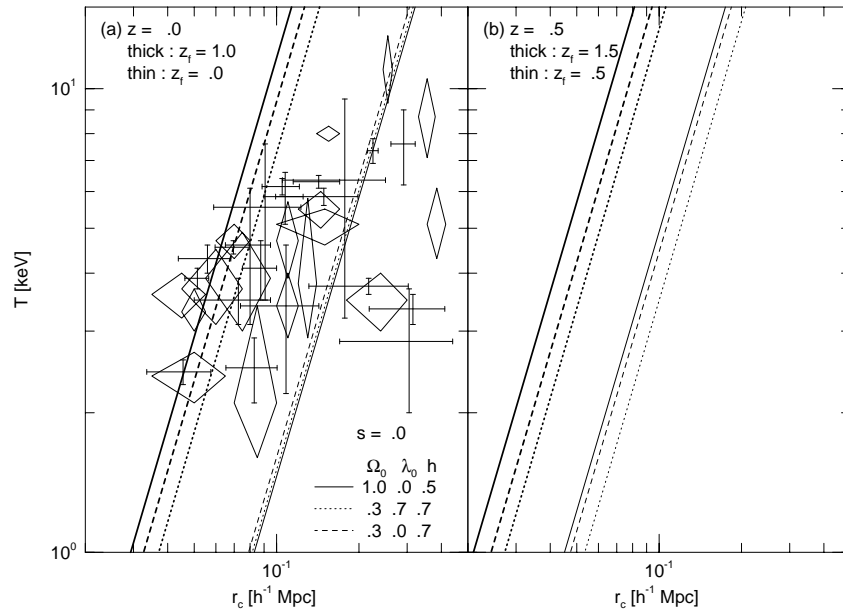


Figure 3: The $T - r_c$ relation for the clusters in CDM models at (a) $z = 0$ and (b) $z = 0.5$. Three representative models, Eh5, L3h7, and O3h7 are plotted in solid, dotted, and dashed lines, respectively. Thick and thin lines correspond to the results for $z_f = z + 1$ and $z_f = z$, respectively. The crosses show the *Einstein* observations (Jones & Forman 1984; David et al. 1993), and the diamonds indicate *EXOSAT* data (Edge & Stewart 1991a,b).

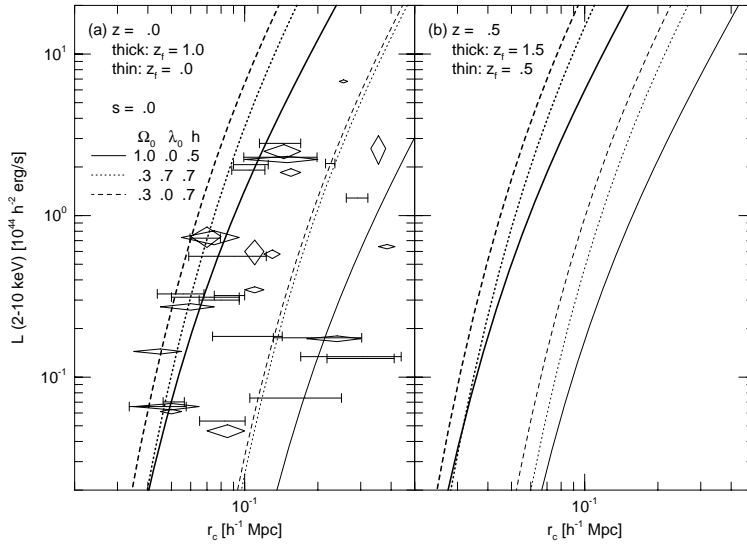


Figure 4: Same as Figure 3 except for the $L(2 - 10\text{keV}) - r_c$ relation.

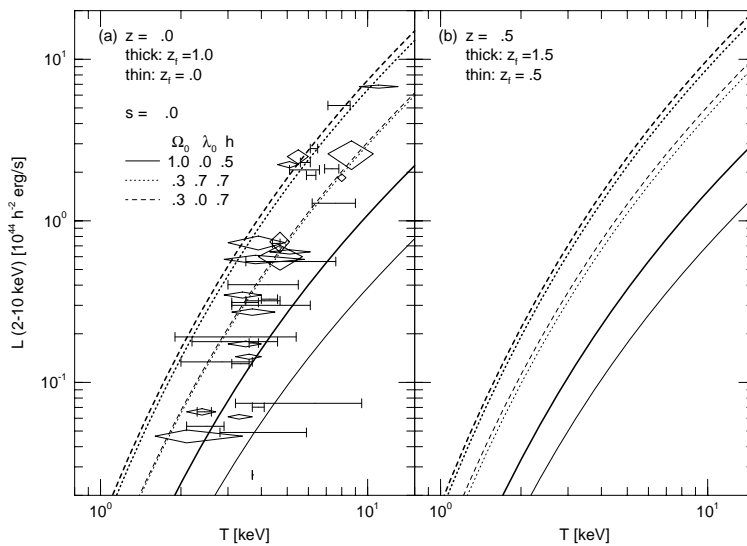


Figure 5: Same as Figure 3 except for the $L(2 - 10\text{keV}) - T$ relation.

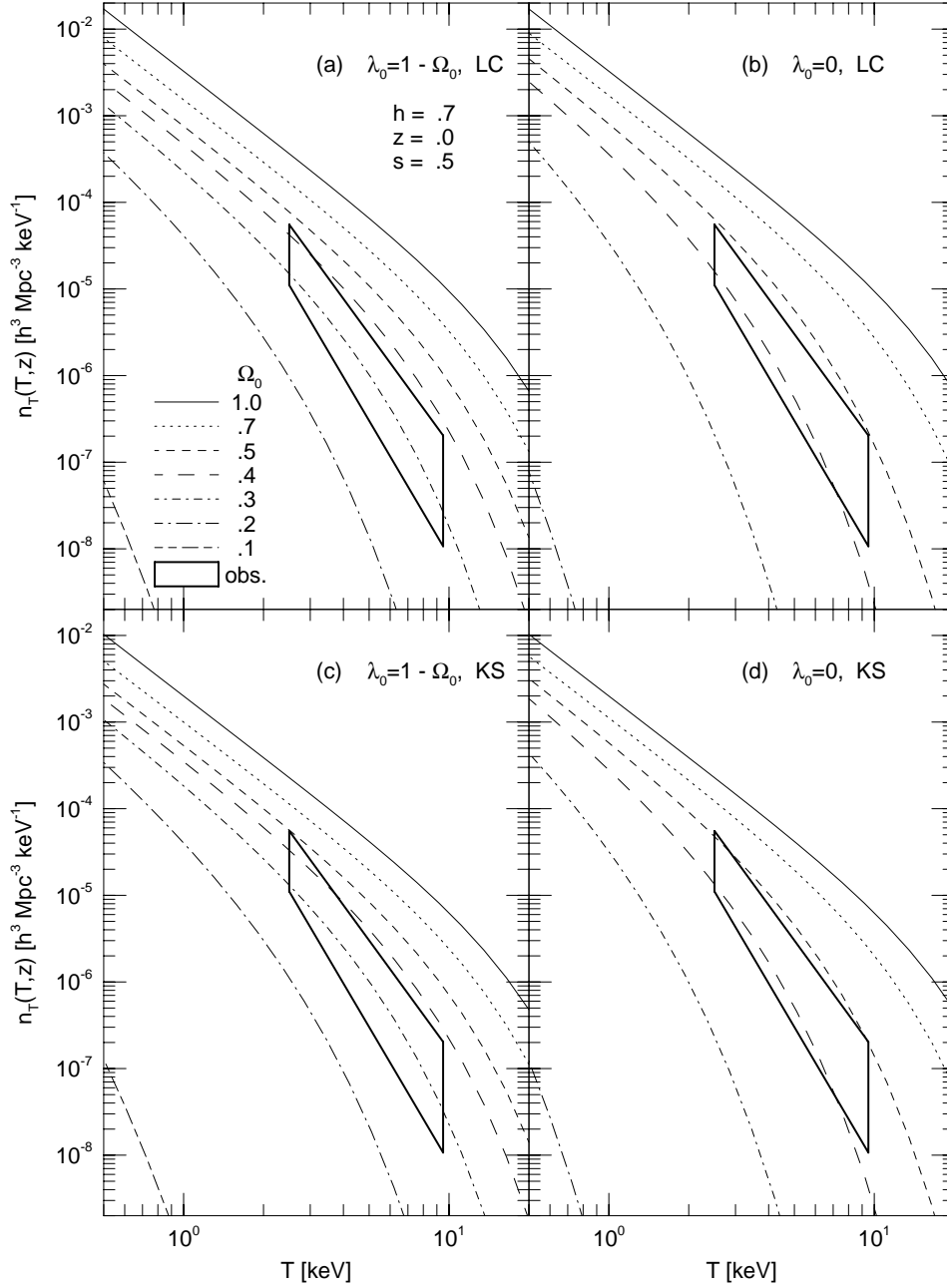


Figure 6: Predictions of the temperature function of clusters at $z = 0$ in CDM universes with $h = 0.7$; (a) LC model with $\lambda_0 = 1 - \Omega_0$, (b) LC model with $\lambda_0 = 0$, (c) KS model with $\lambda_0 = 1 - \Omega_0$, and (d) KS model with $\lambda_0 = 0$. The fluctuation amplitudes are normalized according to the *COBE* 2 year data (Gorski et al. 1995; Sugiyama 1995). The thick solid box indicates the observational error box (Henry & Arnaud 1991).

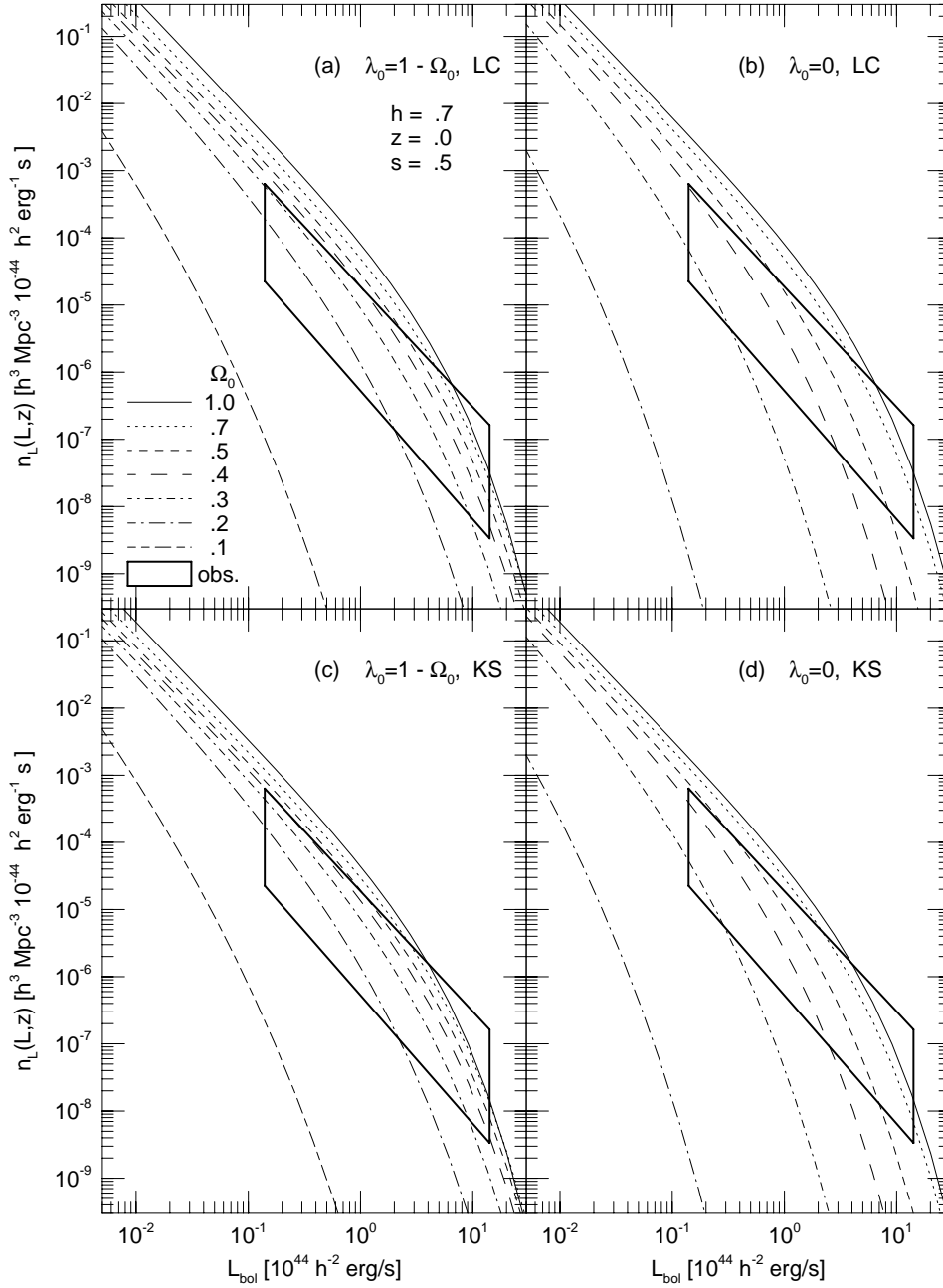


Figure 7: Same as Figure 6 except for the bolometric luminosity function.

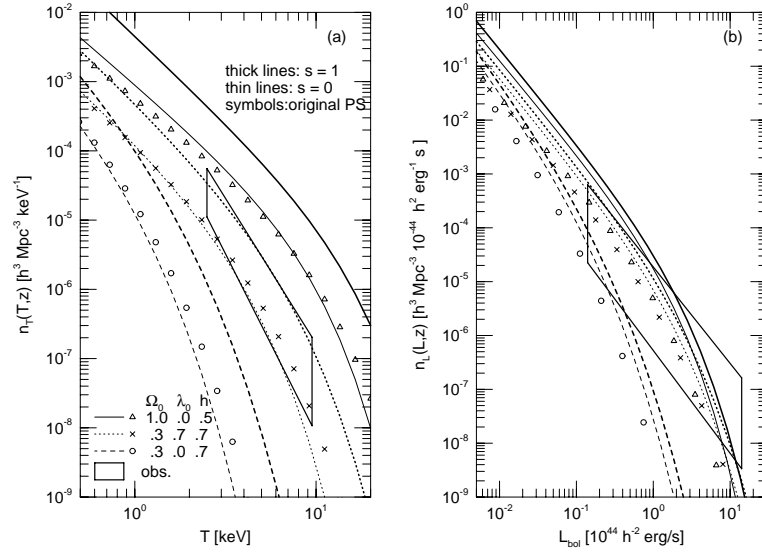


Figure 8: Effect of different evolutionary assumptions on the predictions of (a) temperature and (b) luminosity functions at $z = 0$ in Eh5, L3h7, and O3h7 CDM models (*COBE* normalized). Results for the $s = 1$ and $s = 0$ models are respectively plotted in thick and thin lines, while those based on the original PS model are plotted in symbols.

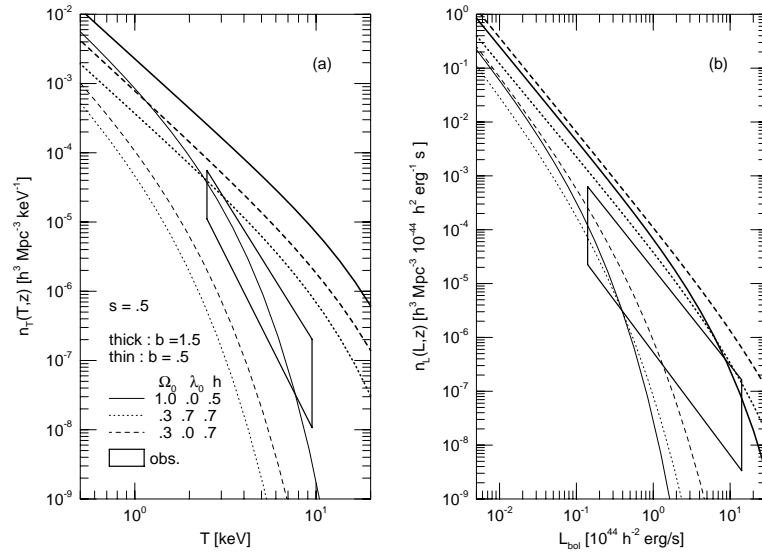


Figure 9: Effect of fluctuation amplitudes on predictions of (a) temperature and (b) luminosity functions at $z = 0$ in Eh5, L3h7, and O3h7 CDM models ($s = 0.5$). Thick and thin lines indicate the results for $b = 1.5$ and $b = 0.5$, respectively.

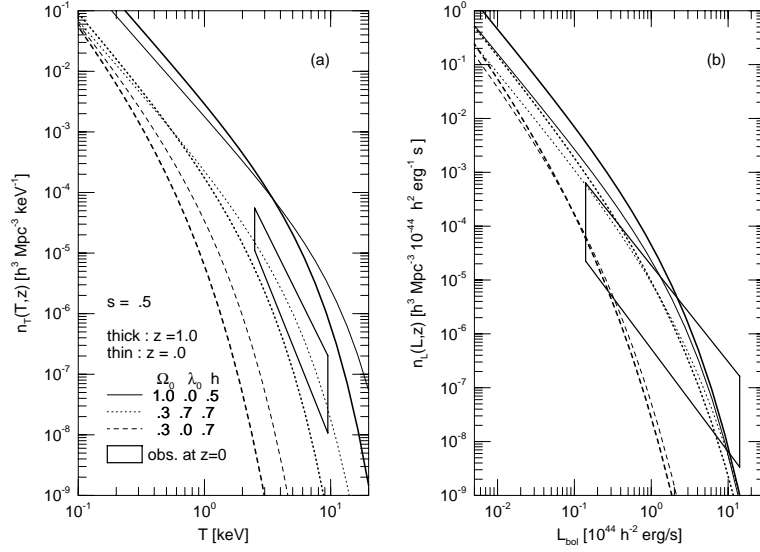


Figure 10: Evolution of (a) temperature and (b) luminosity functions in Eh5, L3h7, and O3h7 CDM models ($s = 0.5$). Thick and thin lines indicate the results for $z = 1$ and $z = 0$, respectively.

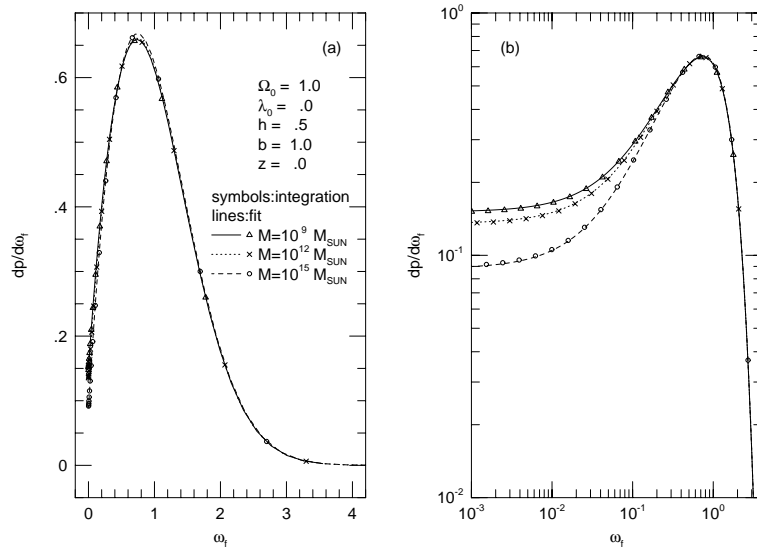


Figure 11: The scaled distribution function of halo formation epochs, $\partial p/\partial\omega_f$, in the standard CDM model ($\Omega_0 = 1$, $\lambda_0 = 0$ and $h = 0.5$); (a) linear and (b) log-log plots. Symbols and lines indicate results of a numerical integration of equation (2.6) and a fit by equations (C.4)–(C.8), respectively; $M = 10^9 M_{\odot}$ (triangles, solid line), $10^{12} M_{\odot}$ (crosses, dotted line), and $10^{15} M_{\odot}$ (circles, dashed line).